Int. J. Electrochem. Sci., 12 **(2017)** 10958 – 10968, doi: 10.20964/2017.11.78

International Journal of
ELECTROCHEMICAL
SCIENCE
www.electrochemsci.org

Electrochemical Synthesis of PtNiCo/3DGN Composite Catalyst and Its Performance for Methanol Electrooxidation

Zhenyu Wang[1], *Feifei Zhang*[1,*], *Qingyun Liu*[2] *and Zonghua Wang*[1]

[1] College of Chemistry and Chemical Engineering, Laboratory of Fiber Materials and Modern Textile, The Growing Base for State Key Laboratory, Shandong Sino-Japanese Center for Collaborative Research of Carbon Nanomaterials, Qingdao University, Qingdao 266071, China
[2] College of Chemistry and Environmental Engineering, Shandong University of Science and Technology, Qingdao 266590, China
[*]E-mail: zhangfeifei00921@126.com

Received: 15 July 2017 / *Accepted:* 16 September 2017 / *Published:* 12 October 2017

A novel PtNiCo/three-dimensional graphene (PtNiCo/3DGN) catalyst was synthesized by sequential electrodeposition of three-dimensional graphene and PtNiCo nanoparticles. The catalysts were characterized by scanning electron microscopy (SEM), transmission electron microscopy (TEM), Raman and electrochemical measurements. Electrochemical experiments revealed that PtNiCo/3DGN catalyst shows high activity for methanol oxidation with improved electrocatalytic capacity (the forward anodic peak current density of 790.4 mA mg_{Pt}^{-1}), which is about 2.02 and 2.06 folds of that for PtNi/3DGN (390.2 mA·mg^{-1}_{Pt}) and PtCo/3DGN (383.9 mA·mg^{-1}_{Pt}), and much higher than Pt (144.0 mA·mg^{-1}_{Pt}) and Pt/3DGN (277.2 mA·mg^{-1}_{Pt}) catalysts.

Keywords: Methanol oxidation; Three-dimensional graphene (3DGN); PtNiCo nanoparticles; Electrodeposition

1. INTRODUCTION

Recently, energy concerns transfer from fossil fuels to new energy resources that are renewable and environmentally benign. In this sense, tremendous effort has been put forward to develop fuel cells, which is a promising power source for portable electronic devices and transportation vehicles.[1-4] Direct methanol fuel cells (DMFCs), one type of fuel cells using liquid methanol as a fuel, has attracted considerable interests due to its high energy conversion efficiency, low operating temperature, less pollutant emission and compactness.[5-8] However, the low catalytic activity of the anode catalysts hinders its commercialization process.[9] In search for efficient Pt based catalysts that

would improve Pt catalytic activity and remedy catalysts poisoning by a carbonaceous inter mediate (most likely CO), many systems have been explored in the form of optimizing the size and shape of Pt nanoparticles, alloying Pt with relatively cheap metals (e.g., Ni[10], Ag[11]and Co[12]) and supporting Pt based nanocatalysts onto nanocarbon materials.

Graphene, a 2D sp^2-hybridized monolayer of graphite, has attracted extensive attention since the discovery of micromechanical cleavage isolated graphene layer from bulk graphite.[13] Graphene has wide potential applications in various fields, such as nanoelectronics,[14] composite materials,[15, 16] energy storage and conversion[17, 18] due to its excellent electrical, mechanical, thermal and optical properties. However, there exist strong π-π interaction between graphene sheets which lead to the irreversible layer-upon-layer aggregate.[19] The aggregation of graphene will reduce the surface area of electrode and hinder the rapid diffusion of electrolyte inside electrodes, consequently decreasing its performance and challenging its practical application. To get around this bottleneck, three-dimensional graphene (3DGN) porous structures and graphene-based composite materials have been widely developed.[20, 21] The three-dimensional architecture material combines the 3D porous structures and the excellent intrinsic properties of graphene, providing with high specific surface areas, highly conductive network and fast mass and electron transport kinetics.[22, 23]

The deleterious effects of Pt catalyst, such as particle aggregation and surface poisoning, cause a decrease of active sites available for the methanol oxidation reaction and sluggish kinetics. Considerable efforts have been taken to alloy Pt with a second metal to build binary catalysts, which contribute to increasing CO tolerance, enhancing catalytic performance and simultaneously reducing the amount of Pt.[11, 24] However, issues such as long-term catalytic durability still hinder the development of DMFCs, where need a functional improvement. In recent years, ternary systems have been investigated as anode electrocatalysts for DMFCs.[25, 26] The addition of the third metal not only improves catalytic activity by the favorable synergistic electronic interaction between Pt and the doped transition metals but also cuts the overall cost of catalysts by reducing the amount of Pt utilized.[27]

Herein we report the fabrication, characterization and electrochemical analyzing of PtNiCo/three-dimensional graphene (PtNiCo/3DGN) catalyst. The fabrication procedure includes three steps. Firstly, 3DGN architecture was deposited onto glassy carbon electrode (3DGN/GCE) by electrochemical reduction of graphene oxide. Secondly, 3DGN/GCE was decorated with Ni and Co via electrochemical deposition (NiCo/3DGN). Thirdly, PtNiCo/3DGN was synthesized by electrodepositing of Pt onto NiCo/3DGN. These procedure were accomplished by electrochemical routes avoiding high temperature and toxic reactants. Moreover, the direct deposition of Pt nanoparticles decorated 3D graphene networks onto the surface of electrodes requires no additional transfer process or binder material, which is attractive for electrochemical application.

2. EXPERIMENTAL

2.1. Chemicals

Graphite powder used for preparation of graphene oxide (GO), was provided by Qingdao Fujin graphite Co., Ltd. (Qingdao, China). $Ni(NO_3)_2{\cdot}6H_2O$, $Co(NO_3)_2{\cdot}6H_2O$, $H_2PtCl_6{\cdot}6H_2O$, CH_3OH and

H_2SO_4 were purchased from Sinopharm Chemical Reagent Co. Ltd. (Shanghai, China). All the reagents were of analytical grade and used without further purification. Doubly distilled water was used throughout the experiment.

2.2. Characterization and electrochemical measurements

The morphologies of the synthesized samples were characterized by scanning electronic microscopy (SEM, JEOL JSM-6700F). The composition of the prepared nanocomposites was evaluated by energy dispersive X-ray analysis (EDS) equipped on the SEM. The structural analysis of the as-prepared catalysts were investigated by X-ray diffraction (XRD, DX2700, China) operating with Cu Kα radition (λ = 1.5418Å). The Raman spectra were obtained with a RAMAN-11 (Nanophoton) with a 532 nm laser source. Electrochemical experiments were performed at a CHI-660B electrochemical workstation (Shanghai Chenhua Instrument Co., Ltd.) with a conventional three-electrode cell. A saturated calomel electrode (SCE), a platinum wire and the modified glassy carbon electrode (GCE) were used as the reference, counter and working electrode, respectively. All the potentials reported in this paper are with respect to this reference electrode.

2.3. Preparation of the modified electrodes

GO was synthesized by using a modified Hummers' method[28]. The 3DGN modified GCE (3DGN/GCE) was prepared by electrolyzing in a 3 mg ml^{-1} GO aqueous suspension, containing 0.1 M lithium perchlorate ($LiClO_4$) in a potential range of -1.5 V- 0.6 V at a scan rate of 25 $mV{\cdot}s^{-1}$. The 3DGN/GCE was further reduced in 1 M $LiClO_4$ aqueous solution to increase its conductivity[19], and washed with doubly distilled water to remove residual $LiClO_4$. The 3DGN/GCE was immersed into a 0.1 M $NaNO_3$ aqueous solution containing different ratios of Ni/Co (molar ratio: 0/1, 1/1, 1/1.5, 1.5/1, 1/2, 2/1, 1/3, 3/1 and 1/0) to get the NiCo/3DGN/GCE, in the potential range from -0.2V to -1.5V at a scan rate of 50 $mV{\cdot}s^{-1}$ [29]. After that, Pt nanoparticles were electrodeposited on the NiCo/3DGN/GCE by cyclic scanning in the potential range from -0.2 V to 1.2 V in 0.038 M H_2PtCl_6 aqueous solution, named as PtNiCo/3DGN/GCE. When the molar ratios of Ni/Co are 0/1 and 1/0, the corresponding electrodes are PtCo/3DGN/GCE and PtNi/3DGN/GCE. For comparison, Pt nanoparticles were also deposited on 3DGN to form Pt/3DGN/GCE.

2.4 Electrocatalytic oxidation of methanol

In order to calculate the electrochemical active surface area (ECSA), the catalytic electrodes were scanned by cyclic voltammetry (CV) in the solution of 0.5 $mol{\cdot}L^{-1}$ H_2SO_4 at a scan rate of 50$mV{\cdot}s^{-1}$. The electrocatalytic oxidation of methanol was studied using CV in the solution of 0.5 $mol{\cdot}L^{-1}$ H_2SO_4 containing 1 $mol{\cdot}L^{-1}$ CH_3OH at a scan rate of 50 $mV{\cdot}s^{-1}$. The stability of different catalysts are investigated by chronoamperometry (CA) method in the solution of 0.5 $mol{\cdot}L^{-1}$ H_2SO_4 containing 1 $mol{\cdot}L^{-1}$ CH_3OH at a fixed potential of 0.70 V.

3. RESULTS AND DISCUSSION

Fig. 1A and 1B present the SEM and TEM image of the 3DGN. It is observed that the electrodeposited graphene constructed a three-dimensional interconnected porous structure, which is beneficial to the loading of catalytic nanoparticles. Compared to 3DGN, it can be seen from Fig. 1C that NiCo composite are successfully incorporated in the interconnected porous 3DGN. The SEM image of PtNiCo/3DGN (Fig. 1D) shown that PtNiCo nanoparticles with size of around 80 nm are uniformly distributed on the 3DGN.

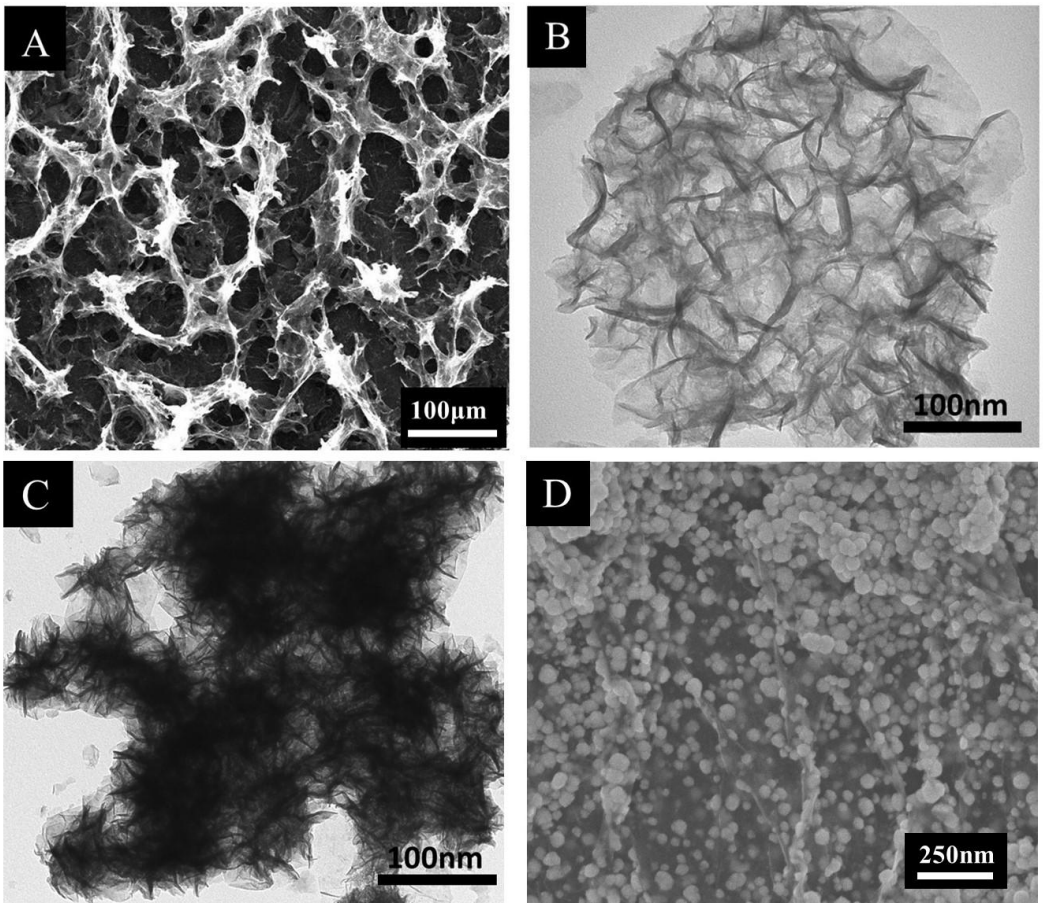

Figure 1. SEM images of 3DGN (A) and PtNiCo/3DGN (D) and TEM images of 3DGN (B) and NiCo/3DGN (C)

The Raman spectra of 3DGN and GO were shown in Fig. 2. They both display strong D (1345 cm^{-1}) bands and G (1585 cm^{-1}) bands originating from carbon sp^2 domains and structural defects [30]. The D band is related to structural defects in the curved graphene sheet or partially disordered structures of graphitic domains, while the G band corresponds to the graphitic hexagon-pinch pattern. The D/G intensity ratio increases from GO to 3DGN, suggesting a decrease in average size of the graphitic domain in the process of the electrochemical reduction, probably due to the formation of new sp^2 domains that were smaller in size but larger in quantity[31].

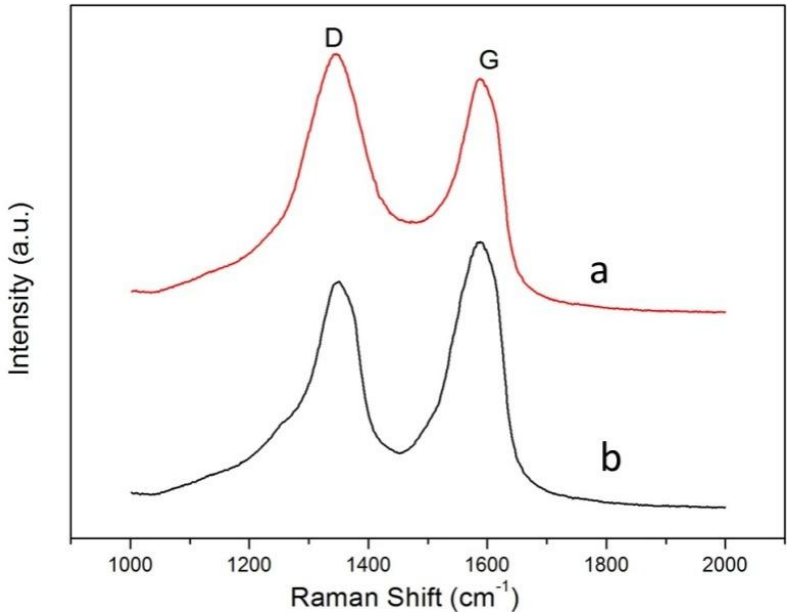

Figure 2. Raman spectra of 3DGN (a) and GO (b).

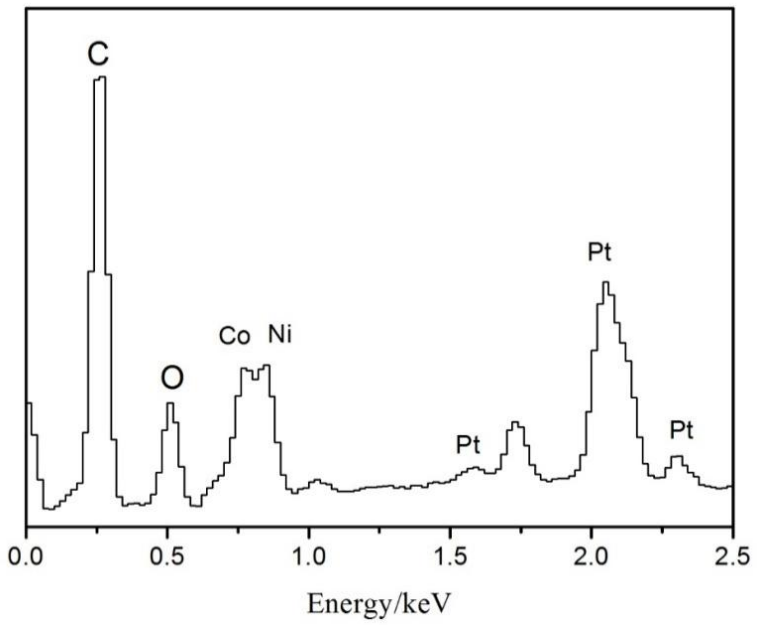

Figure 3. The EDS spectrum of PtNiCo/3DGN composite. (Ni/Co=1/1)

The EDS spectrum shown in Fig. 3 further verifies that the composite mainly includes five kinds of elements, C, O, Co, Ni and Pt. The ratio of Ni and Co mass percentage is about 1:1, which is in accordance with the proportion of the two elements in the precursor solution. According to the EDS spectrum, the comparison of different molar ratios of Ni and Co in precursor is shown in Table 1. It can be seen that different PtNiCo/3DGN composites are almost identical with the precursor molar ratios of Ni and Co.

Table 1. The comparison of Ni and Co with different molar ratios in precursor with corresponding EDS results.

The precursor molar ratios of Ni and Co	The results of EDS
1.0:1.0	1:0.94
1.0:1.5	1:1.63
1.0:2.0	1:1.89
1.0:3.0	1:3.18
1.5:1.0	1.46:1
2.0:1.0	2.15:1
3.0:1.0	2.76:1

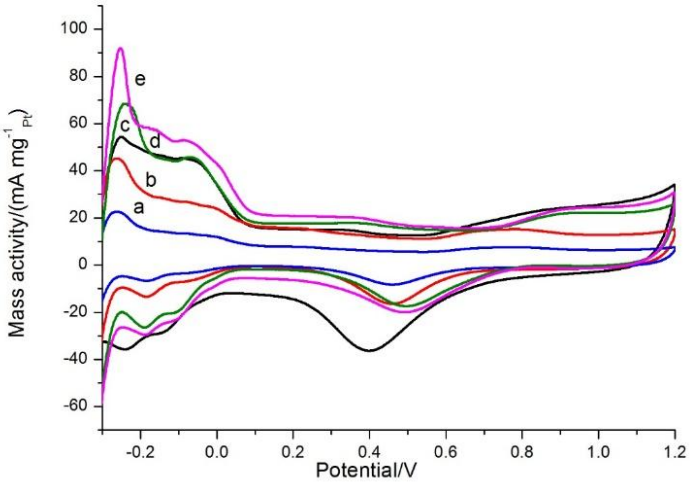

Figure 4. CV curves of Pt (a), Pt/3DGN (b), PtCo/3DGN (c), PtNi/3DGN (d) and PtNiCo/3DGN (e) modified electrodes in the solution of 0.5 mol·L^{-1} H_2SO_4 at a scan rate of 50mV·s^{-1}

Fig.4 shows CVs of Pt, Pt/3DGN, PtCo/3DGN, PtNi/3DGN and PtNiCo/3DGN modified electrodes in the solution of 0.5 mol·L^{-1} H_2SO_4 at a scan rate of 50mV·s^{-1}. The ECSA could be estimated from columbic charge (Q_H) for hydrogen adsorption and desorption obtained from CV curves between -0.2 V and 0.0 V, in the solution of 0.5 mol·L^{-1} H_2SO_4. According to the equation ECSA= Q_H/ (210m_{Pt}), where m_{Pt} represents the electrode loading of Pt. The peak of hydrogen adsorption was higher for PtNiCo/3DGN catalyst than Pt, Pt/3DGN, PtCo/3DGN and PtNi/3DGN catalysts. This result can be interpreted as the synergistic effect between Pt, Ni, Co and graphene [32]. The ECSA is measured to be Pt (25.97 $m^2 \cdot g^{-1}$), Pt/3DGN (51.94 $m^2 \cdot g^{-1}$), PtCo/3DGN (80.28 $m^2 \cdot g^{-1}$), PtNi/3DGN (84.88 $m^2 \cdot g^{-1}$) and PtNiCo/3DGN (100.26 $m^2 \cdot g^{-1}$). The high ECSA obtained from PtNiCo/3DGN catalyst is contributed to the uniform loading of catalytic nanoparticles on the 3DGN nanoporous structure. It implies that there are more active sites available for methanol on the surface of PtNiCo/3DGN catalyst [33].

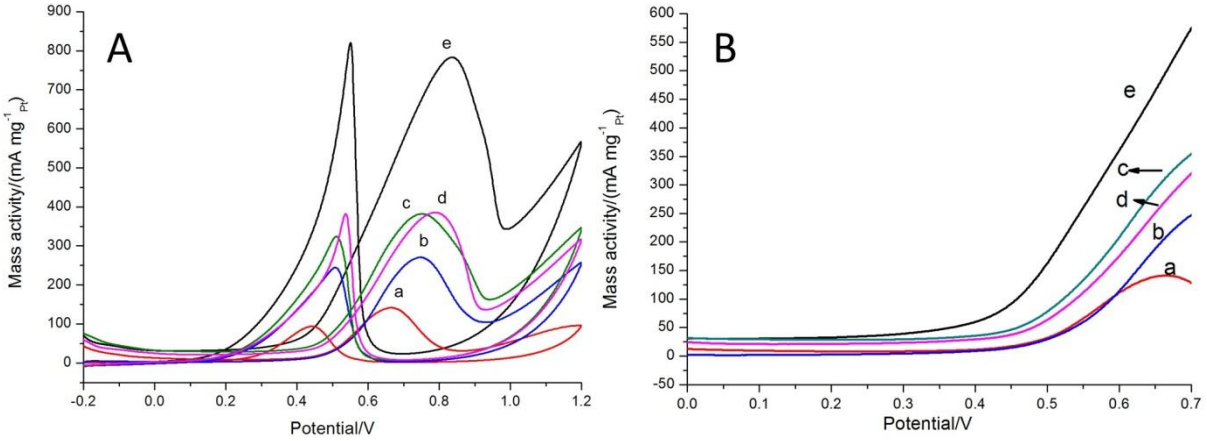

Figure 5 (A) CV curves of Pt (a), Pt/3DGN (b), PtNi/3DGN (c), PtCo/3DGN (d) and PtNiCo/3DGN (e) in the solution of 0.5 mol·L^{-1} H_2SO_4 containing 1 mol·L^{-1} CH_3OH at a scan rate of 50 mV·s^{-1}; (B) The partial magnification of the CVs in a potential of 0.0- 0.7 V.

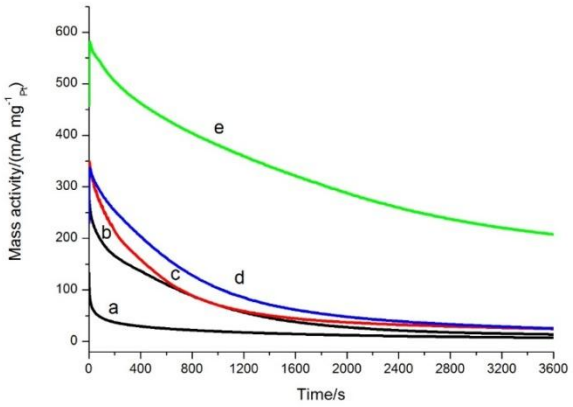

Figure 6 CA curves for Pt (a), Pt/3DGN (b), PtCo/3DGN (c), PtNi/3DGN (d) and PtNiCo/3DGN (e) in the solution of 0.5 mol·L^{-1} H_2SO_4 containing 1 mol·L^{-1} CH_3OH at a fixed potential of 0.70 V.

The electrocatalytic properties of different composite catalysts toward methanol electrooxidation are investigated in the solution of 0.5 mol·L^{-1} H_2SO_4 containing 1 mol·L^{-1} CH_3OH at a scan rate of 50 mV·s^{-1}. As shown in Fig. 5A, there are two oxidation peaks being observed. The strong current density peak in the forward scan at about 0.8 V is attribute to the methanol oxidation. The higher current density peak, the larger extent of methanol oxidation, the higher electrocatalytic property of catalyst [34]. When the potential scan is reversed, another current density peak at about 0.4 V is due to the oxidation of COads-like species which generated from the incomplete oxidation of methanol during the forward potential scan [35]. The height of this peak depends on the capacity of the residual poisoning species that can be removed [36]. The PtNiCo/3DGN (a) gives a mass activity of 790.4 mA·mg$^{-1}_{Pt}$, which is about 2.02 and 2.06 fold of that of PtNi/3DGN (c, 390.2 mA·mg$^{-1}_{Pt}$) and PtCo/3DGN (d, 383.9 mA·mg$^{-1}_{Pt}$), far higher than Pt (a, 144.0 mA·mg$^{-1}_{Pt}$) and Pt/3DGN (b, 277.2 mA·mg$^{-1}_{Pt}$) modified electrodes. Fig. 5B shows that the onset potential for Pt, Pt/3DGN, PtNi/3DGN,

PtCo/3DGN and PtNiCo/3DGN are 0.45 V, 0.44 V, 0.43 V, 0.42 V and 0.33 V, respectively, which indicating that it is more favorable for methanol oxidation on PtNiCo/3DGN catalyst.

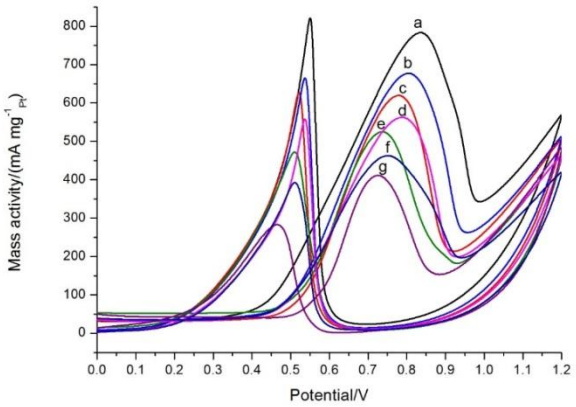

Figure 7 CV curves of PtNiCo/3DGN with different Ni/Co ratios in the solution of 0.5 mol·L^{-1} H_2SO_4 containing 1 mol·L^{-1} CH_3OH at a scan rate of 50 mV·s^{-1} with a) 1/1, b) 1/1.5, c) 1.5/1, d) 1/2, e) 2/1, f) 1/3, g) 3/1.

To evaluate the status of surface poisoning, CA curves of Pt (a), Pt/3DGN (b), PtCo/3DGN (c), PtNi/3DGN (d) and PtNiCo/3DGN (e) are measured in the solution of 0.5 mol·L^{-1} H_2SO_4+ 1 mol·L^{-1} CH_3OH (Fig. 6). The potential is held at 0.70 V during the measurements. The PtNiCo/3DGN catalyst exhibits slowest current density degradation over time compared to other four kinds of catalysts, in the meanwhile, performs a highest tolerance to the intermediate poisoning species during the oxidation process of methanol. It can also be observed that the PtNiCo/3DGN catalyst presents a higher current density than that of other catalysts, demonstrating that the PtNiCo/3DGN catalyst is more active for electrooxidation of methanol.

Table 2. Comparison of our work with other reported works on the catalytic activity for methanol oxidation.

Catalyst	ECSA (m^2 g_{Pt}^{-1})	Mass activity (mA mg_{Pt}^{-1})	Ref.
Pt/PB/graphene	85.7	445.0	[37]
PtNi/graphene	-	370.0	[38]
Pt-Ru/VG	-	339.2	[39]
PtPd NW/RGO	23.0	510.0	[40]
Pt-CeO_2/RGO	18.0	194.5	[41]
PtNiCo/3DGN	100.26	790.4	This work

The influence of Ni/Co ratio for electrooxidation of methanol is investigated by CV method in the solution of 0.5 mol·L^{-1} H_2SO_4 containing 1 mol·L^{-1} CH_3OH. It can be observed from Fig. 7 that the PtNiCo/3DGN catalyst with Ni/Co ratio of 1/1 possesses of a maximum current density, significantly higher than those of other six kinds of catalysts and thus indicating that the Ni/Co ratio of 1/1 is an optimum ratio for PtNiCo/3DGN catalyst.

For further evaluating the performance of the as prepared PtNiCo/3DGN catalyst, some relevant reported works have been generalized in Table 2 for comparison. Compared to many relevant works, our PtNiCo/3DGN catalyst shows larger ECSA, better catalytic performance and higher stability for methanol oxidation.

To evaluate of the activity and stability of different catalysts, CA curves are recorded for a period of time (3600s) for the oxidation of methanol (Fig. 8). The results shown that the highest methanol current density is obtained on the PtNiCo/3DGN catalyst with Ni/Co ratio of 1/1, which are consistent with the CV results observed in Fig. 7. The PtNiCo/3DGN catalyst also exhibits a slowest current degradation among all the catalysts, that indicating an excellent tolerance to the poisoning species.

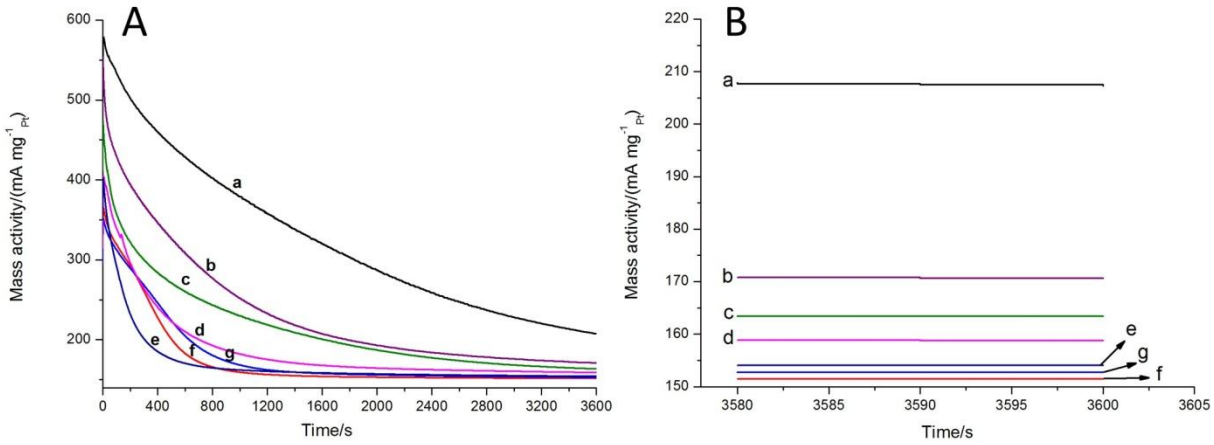

Figure 8 (A) CA curves of PtNiCo/3DGN with different Ni/Co ratios: a) 1/1, b) 1/1.5, c) 1.5/1, d) 1/2, e) 2/1, f) 1/3, g) 3/1. (B) The partial magnification of CA curves in the time range of 3580s to 3600s. The test is performed in a 0.5 mol·L^{-1} H_2SO_4 containing 1 mol·L^{-1} CH_3OH at a fixed potential of 0.70 V.

4. CONCLUSION

We have developed a facile procedure to synthesize PtNiCo/3DGN composite catalyst. 3DGN, as the support for catalyst particles, efficiently improves electroactive for methanol oxidation reaction. The addition of Ni and Co further enhanced the catalytic activity, stability and tolerance to poisoning species which generated during the methanol oxidation reaction. The influence of Ni/Co ratio in the composite catalyst on electrocatalytic activity for methanol oxidation reaction is investigated. The results show when the ratio of Ni/Co is 1/1, the PtNiCo/3DGN catalyst has the optimal performance.

ACKNOWLEDGMENTS
This work was supported by the National Natural Science Foundation of China (21405086, 21475071), the Taishan Scholar Program of Shandong Province and Postdoctoral Foundation of Qingdao (2015113).

References

1. Y.J. Hu, P. Wu, Y.J. Yin, H. Zhang, C.X. Cai, *Appl. Catal. B-Environ.*, 111 (2012) 208.
2. X.T. Chen, Y.Y. Jiang, J.Z. Sun, C.H. Jin, Z.H. Zhang, *J. Power Sources*, 267 (2014) 212.
3. M.J. Wang, X.F. Song, Q. Yang, H. Hua, S.G. Dai, C.G. Hu, D.P. Wei, *J. Power Sources*, 273 (2015) 624.
4. Y.H. Xiao, Z.G. Fu, G.H. Zhan, Z.C. Pan, C.M. Xiao, S.K. Wu, C. Chen, G.H. Hu, Z.G. Wei, *J. Power Sources*, 273 (2015) 33.
5. G. Shi, Z. Wang, J. Xia, S. Bi, Y. Li, F. Zhang, L. Xia, Y. Li, Y. Xia, L. Xia, *Electrochim Acta*, 142 (2014) 167.
6. M. Zhiani, B. Rezaei, J. Jalili, *Int. J. Hydrog. Energy*, 35 (2010) 9298.
7. X.L. Wang, C. Li, G.Q. Shi, *Phys. Chem. Chem. Phys*., 16 (2014) 10142.
8. M.K. Jeon, P.J. McGinn, *J. Power Sources*, 188 (2009) 427.
9. S. Yu, Q. Liu, W. Yang, K. Han, Z. Wang, H. Zhu, *Electrochim. Acta*, 94 (2013) 245.
10. L. Li, Y. Wu, J. Lu, C. Nan, Y. Li, *Chem. Commun.*, 49 (2013) 7486.
11. J.Y. Cao, M.W. Guo, J.Y. Wu, J. Xu, W.C. Wang, Z.D. Chen, *J. Power Sources*, 277 (2015) 155.
12. G. Shi, Z. Wang, J. Xia, F. Zhang, Y. Xia, Y. Li, *Acta Chim Sinica*, 71 (2013) 227.
13. K.S. Novoselov, A.K. Geim, S.V. Morozov, D. Jiang, Y. Zhang, S.V. Dubonos, I.V. Grigorieva, A.A. Firsov, *Science*, 306 (2004) 666.
14. R. Singh, D. Kumar, C.C. Tripathi, *Indian Journal of Pure & Applied Physics*, 53 (2015) 501.
15. C.-C. Wang, S.-Y. Lu, *Nanoscale*, 7 (2015) 1209.
16. P. Wei, M. Fan, H. Chen, D. Chen, C. Li, K. Shu, C. Lv, *Int. J. Hydrog. Energy*, 41 (2016) 1819.
17. Z.-L. Wang, D. Xu, H.-G. Wang, Z. Wu, X.-B. Zhang, *ACS Nano*, 7 (2013) 2422.
18. L. Dai, *Accounts of Chemical Research*, 46 (2013) 31.
19. K. Chen, L. Chen, Y. Chen, H. Bai, L. Li, *Journal of Materials Chemistry*, 22 (2012) 20968.
20. G. Zhou, Z. Ye, W. Shi, J. Liu, F. Xi, *Progress in Chemistry*, 26 (2014) 950.
21. Y. Ma, Y. Chen, *National Science Review*, 2 (2015) 40.
22. Y. Zhao, C.G. Hu, L. Song, L.X. Wang, G.Q. Shi, L.M. Dai, L.T. Qu, *Energy Environ. Sci*., 7 (2014) 1913.
23. C. Li, G.Q. Shi, *Nanoscale*, 4 (2012) 5549.
24. J.N. Zheng, L.L. He, C. Chen, A.J. Wang, K.F. Ma, J.J. Feng, *J. Power Sources*, 268 (2014) 744.
25. J. Zeng, J.Y. Lee, Ruthenium-free, *Int. J. Hydrog. Energy*, 32 (2007) 4389.
26. A. Papaderakis, N. Pliatsikas, C. Prochaska, K.M. Papazisi, S.P. Balomenou, D. Tsiplakides, P. Patsalas, S. Sotiropoulos, *Frontiers in Chemistry*, 2 (2014)29.
27. M.E. Scofield, C. Koenigsmann, L. Wang, H. Liu, S.S. Wong, *Energy Environ. Sci*., 8 (2015) 350.
28. Z. Wang, Q. Han, J. Xia, L. Xia, M. Ding, J. Tang, *Journal of Separation Science*, 36 (2013) 1834.
29. M. Yang, H. Cheng, Y. Gu, Z. Sun, J. Hu, L. Cao, F. Lv, M. Li, W. Wang, Z. Wang, S. Wu, H. Liu, Z. Lu, *Nano Res.*, 8(2015) 2744.
30. R. Beams, L.G. Cancado, L. Novotny, *J. Phys.-Condes*. Matter 27 (2015) 083002.
31. F.F. Zhang, J. Tang, N. Shinya, L.C. Qin, *Chem. Phys. Lett.* 584 (2013) 124.
32. W.F. Xie, F.F. Zhang, Z.H. Wang, M. Yang, J.F. Xia, R.J. Gui, Y.Z. Xia, *J. Electroanal. Chem.* 761 (2016) 55.
33. R.P. Xiu, F.F. Zhang, Z.H. Wang, M. Yang, J.F. Xia, R.J. Gui, Y.Z. Xia, *Rsc Adv* 5 (2015) 86578.
34. Y. Zhang, G. Chang, H. Shu, M. Oyama, X. Liu, Y. He, *J Power Sources* 262 (2014) 279.

35. M.S. Wietecha, J. Zhu, G. Gao, N. Wang, H. Feng, M.L. Gorring, M.L. Kasner, S. Hou, *J Power Sources* 198 (2012) 30.
36. B. Habibi, M.H. Pournaghi-Azar, H. Abdolmohammad-Zadeh, H. Razmi, *Int. J. Hydrog. Energy* 34 (2009) 2880.
37. Z. Wang, G. Shi, J. Xia, Y. Xia, F. Zhang, L. Xia, D. Song, J. Liu, Y. Li, L. Xia, M.E. Brito, *Electrochim Acta*, 121 (2014) 245.
38. Y. Hu, P. Wu, Y. Yin, H. Zhang, C. Cai, Applied Catalysis *B: Environmental*, 111 (2012) 208.
39. Z. Bo, D. Hu, J. Kong, J. Yan, K. Cen, *J Power Sources*, 273 (2015) 530.
40. S. Du, Y. Lu, R. Steinberger-Wilckens, *Carbon*, 79 (2014) 346.
41. X. Yu, L. Kuai, B.Y. Geng, *Nanoscale*, 4 (2012) 5738.